Nano Energy 96 (2022) 107073

Contents lists available at ScienceDirect

Nano Energy

journal homepage: www.elsevier.com/locate/nanoen

Flexible six-dimensional force sensor inspired by the tenon-and-mortise structure of ancient Chinese architecture for orthodontics

Jiahui Hu [a,b,c,1], Ye Qiu [a,b,c,1], Xueer Wang [d], Lelun Jiang [e], Xiaoyan Lu [f], Ming Li [g], Zhiqiang Wang [a,b,c], Kai Pang [h], Ye Tian [a,b,c], Wenan Zhang [d], Zhen Xu [h], Hengjie Zhang [a,b,c], Hangcheng Qi [a,b,c], Aiping Liu [i], Zheng Zhang [a,b,c], Huaping Wu [a,b,c,*]

[a] College of Mechanical Engineering, Zhejiang University of Technology, Hangzhou 310023, China
[b] Key Laboratory of Special Purpose Equipment and Advanced Processing Technology, Ministry of Education and Zhejiang Province, Zhejiang University of Technology, Hangzhou 310023, China
[c] Collaborative Innovation Center of High-end Laser Manufacturing Equipment (National "2011 Plan"), Zhejiang University of Technology, China
[d] College of Information Engineering, Zhejiang University of Technology, Hangzhou 310023, China
[e] Guangdong Provincial Key Laboratory of Sensor Technology and Biomedical Instrument, School of Biomedical Engineering, Shenzhen Campus of Sun Yat-sen University, Shenzhen 518107, China
[f] School of Civil Engineering, Harbin Institute of Technology, Harbin 150001, China
[g] State Key Laboratory of Structural Analysis for Industrial Equipment, Dalian University of Technology, Dalian 116024, China
[h] Department of Polymer Science and Engineering, Zhejiang University, 38 Zheda Road, Hangzhou 310027, China
[i] Center for Optoelectronics Materials and Devices, Zhejiang Sci-Tech University, Hangzhou 310018, China

ARTICLE INFO

Keywords:
Six-dimensional force
Tenon-and-mortise structure
Deep neural networks
Orthodontic

ABSTRACT

Precise multi-axis operation is essentially required in orthodontics for tooth movement. Despite the development of flexible multi-dimensional force sensors that have effectively perceived multi-dimensional forces, they still face the challenge of simultaneously 3D force and moment in a single flexible force sensor. Six-dimensional force perception can successfully operate objects that critically rely on directional tracking and accurate monitoring of complex multi-axis stimuli. To realize the integration of sensing units with the perception of six-dimensional force under even a soft touch, we design a flexible six-dimensional force sensor with tenon-and-mortise interlocking structures inspired by traditional Chinese ancient architecture. This unique structure enables conjunction of deformation, which can be studied and decoded by Deep Neural Networks (DNN) with six-dimensional force, including forces and rotating moments in the x, y, and z directions. This soft sensor with minimal size ($7 \times 7 \times 7$ mm^3) and high detection accuracy (the DNN error is below 10^{-4}) can be used in orthodontic treatment for precise correction with a full collection of orthodontic force. This unique flexible six-dimensional force sensor provides a new strategy for the design of multi-dimensional force sensors, paving the way for the development of intelligent robotics, interactive human-machine interfacing, and advanced prosthetics.

1. Introduction

Wearable sensors have attracted great interest because of their promising applications in human health surveillance and robotics [1–13]. Flexible tactile sensors have been proposed that take advantage of novel materials and designs of micro/nanostructures based on piezoresistive [14–17], capacitive [18], triboelectric [19], and piezoelectric [20–23] sensing mechanisms. These sensing schemes are sensitive to various stimuli, including normal force [24,25], shear force [26,27], strain [28–31], etc. However, tactile sensing is required for precision manipulation tasks to provide feedback information of force and moment in the x, y, and z directions. For instance, orthodontics requires forces and moments to accomplish the task of moving and rotating the teeth. Thus, developing flexible tactile sensors with six-dimensional force sensing capability is highly desirable for future medical surgery.

Although six-dimensional force perception is possible using rigid materials [32–37], they are hard to adapt to the various deformations of soft interfaces. Remarkable progress has been made for flexible sensors

* Corresponding author at: College of Mechanical Engineering, Zhejiang University of Technology, Hangzhou 310023, China.
E-mail address: hpwu@zjut.edu.cn (H. Wu).
[1] J. H. Hu and Y. Qiu contributed equally to this work.

https://doi.org/10.1016/j.nanoen.2022.107073
Received 14 December 2021; Received in revised form 13 February 2022; Accepted 16 February 2022
Available online 22 February 2022

with extended capabilities to detect various stimuli [38–42]. Multi-dimensional force perception was realized by introducing interlocking microstructures into the design of sensing schemes, such as columns [43], fibers [44,45], and hemispheres [46] microstructures. The contact area induced by the microstructures deformation experiences distinct change and provides strain information for identifying the external loads. Nevertheless, the distinction of different stimuli depends on the changing trend of the sensing signal, thus making it difficult to solve signal coupling to detect external stimuli further quantitatively. To address the problem of quantitative identification of multi-dimensional force, additional efforts on the multi-dimensional force sensing have been explored by using anisotropic materials [47–54] or adding unique bump structures [55–61]. The former relies on the differential sensitivity of materials to stimuli in different directions to perceive multi-dimensional forces, whereas the latter responds to multi-dimensional stimuli via the sensing arrays integrated on the substrate with bump structures. However, these studies are limited to efficiently decoding three-dimensional spatial force and lack the perception of torque from physical stimuli.

Therefore, it's still a challenge to enable six-dimensional force sensing using flexible materials, which requires the design of a unique structure to achieve six-dimensional force sensing and reduce the mutual coupling of six-dimensional force signals. Here, we propose a six-dimensional force sensor inspired by the tenon-and-mortise structure of traditional Chinese ancient buildings. The upper and lower bases of the flexible sensor with concave and convex interlocking structures provide a unique strategy to develop sensing modules responsive to external stimuli in six directions (i.e., *Fx*, *Fy*, *Fz*, *Mx*, *My*, *Mz*). The designed structure allows the flexible sensor to associate external stimuli with sensing signals, thus further quantitatively perceiving the six-dimensional force. The force information can be mapped and calibrated by using the Deep Neural Networks (DNN), and the DNN error is below 10^{-4}. Thus, our flexible six-dimensional force sensor can provide more force sensing information than existing works to quantitatively detect complex external stimuli (Table S1, Supporting Information). As a proof-of-concept demonstration, the flexible six-dimensional force sensor is successfully integrated with braces to collect the magnitude and direction of the orthodontic force during different stages in orthodontic treatment. It is helpful for dentists to realize the force information of teeth in various postures to reduce orthodontics' side effects and treatment cycle.

2. Results and discussion

2.1. Conception design of the flexible six-dimensional force sensor

The tenon-and-mortise structure existed commonly in ancient Chinese buildings, providing tight interlock instead of screws. The recessed part is called mortise, and the protruding portion is called tenon (Fig. 1a). This unique structure allows a certain amount of deformation in case of various loading conditions. Incorporating this structure with flexible sensors, we built a flexible tactile sensor that can sense six-dimensional force.

This work improved the previous graphic design thinking of flexible tactile sensors and rationally arranged the sensing unit in three-dimensional space through the tenon-and-mortise base so that the flexible six-dimensional force sensor can have a unique signal response in various deformations of the tenon-and-mortise base. The concave part of the sensor base is the mortise substrate, and the protruding part of the base is the tenon substrate (Fig. 1b). The force-sensing layer is folded 90° along the small hole and bonded to the tenon substrate by adhesive, followed by the acrylic tape to the mortise substrate. When the six-dimensional tactile sensor is in different directions of stimulation, contact deformation occurs between mortise substrate and tenon substrate, squeezing the middle force sensing layer. The 12 pressure-sensitive conductive sheets evenly distributed on the FPCB (flexible printed circuit board, Figure. S1, Supporting Information) are deformed accordingly. This allows for the detection of six-dimensional forces through the different signal response forms of the 12 sensing units. The sensor can be made to the size of a fingertip ($7 \times 7 \times 7$ mm^3), and the sensing unit has good performance (Figure. S2, Supporting Information), which can be ideally used in human health monitoring and advanced prosthetics (Fig. 1c).

For example, in orthodontics, malocclusion needs to be corrected by applying orthodontic force. The six-dimensional tactile sensor installed between the tooth and the braces maps the 12 channel voltage signals detected in the orthodontic process to the six-dimensional forces (F_x, F_y, F_z, M_x, M_y, M_z) through the DNN. It can help dentists know the orthodontic force acting on the tooth surface and conduct orthodontics (Fig. 1d). Therefore, this work has made a detailed exploration of the six-dimensional tactile sensor's action mechanism and performance parameters.

2.2. Deformation mode of the flexible six-dimensional force sensor

The six-dimensional force-sensing capability of the flexible sensor lies in the unique tenon-and-mortise structure (Figure. S4, Supporting Information), which provides a strategy to generate various contact deformation modes under the external stimuli in different directions (Fig. 2a). In different deformation modes, the 12 sensing units in the force sensing layer produce a change in the voltage signal in response. The external stimulus is precisely detected by the corresponding form of voltage signal change.

To demonstrate the superiority of tenon-and-mortise structure in the flexible six-dimensional force sensor. This work qualitatively elucidates the sensing mechanism of the flexible six-dimensional force sensor through a complete set of numerical design tools and experimental test protocols (Note S1, Supporting Information). The axes established in the sensor are shown in Fig. S3. The finite element analysis results show that the mortise base of the sensor moves vertically downward while the vertical pressure is applied (Fig. 2a-I) and further squeezes the four horizontally placed sensing units above the tenon base (Fig. 2b-I). The stress distributions of the sensor indicate that four horizontally placed sensing units are deformed with the applied pressure (Fig. 2c-I). The experimental measurement is further carried out to explore the voltage signal response, which agrees reasonably well with results from finite element analyses and the sensing units S3, S6, S9, and S12 respond (Fig. 2d-I). Besides, the mortise substrate of the sensor is displaced laterally under the lateral force (Fig. 2a-II), and two feet squeeze the piezoresistive sensing unit placed longitudinally on the corresponding side (Fig. 2b-II). Two longitudinally placed sensing units, S1 and S5 on the left, are squeezed (Fig. 2c-II), leading to a tangential pressure-induced voltage response (Fig. 2d-II). Note: Lateral force F_x and F_y deformation patterns are the same, and the response of the sensing unit is different. The responses for F_x (+) are S1 and S5, and for F_y (+) are S4 and S8.

Compared to the pressure-responsive behavior, the deformed form of the sensor is more complicated and changeable (Fig. 2a-III and a-IV). The mortise substrate rotates around the z-axis of the sensor after the applied moment in the positive direction of the z-axis, whereas the tenon substrate remains stable (Fig. 2b-III). The four legs of the mortise base squeeze the vertical sensing unit in a counterclockwise direction, causing the sensing units S2, S5, S8, and S11 to generate voltage signals (Fig. 2c-III and d-III). The finite element analysis results show that the mortise substrate rotates laterally with respect to the tenon substrate when the sensor is subjected to lateral torque (Fig. 2b-IV). After applying lateral torque to the sensor through finite elements and experiments, it was found that the mortise substrate rotated laterally relative to the tenon substrate, squeezing the corresponding sensing units S1, S5, and S9 (Fig. 2c-IV and d-IV). Note: Lateral torque M_x and M_y deformation patterns are the same, and the response of the sensing unit is different. The responses for M_x (+) are S2, S6, and S10, and for M_y (+) are S1, S5,

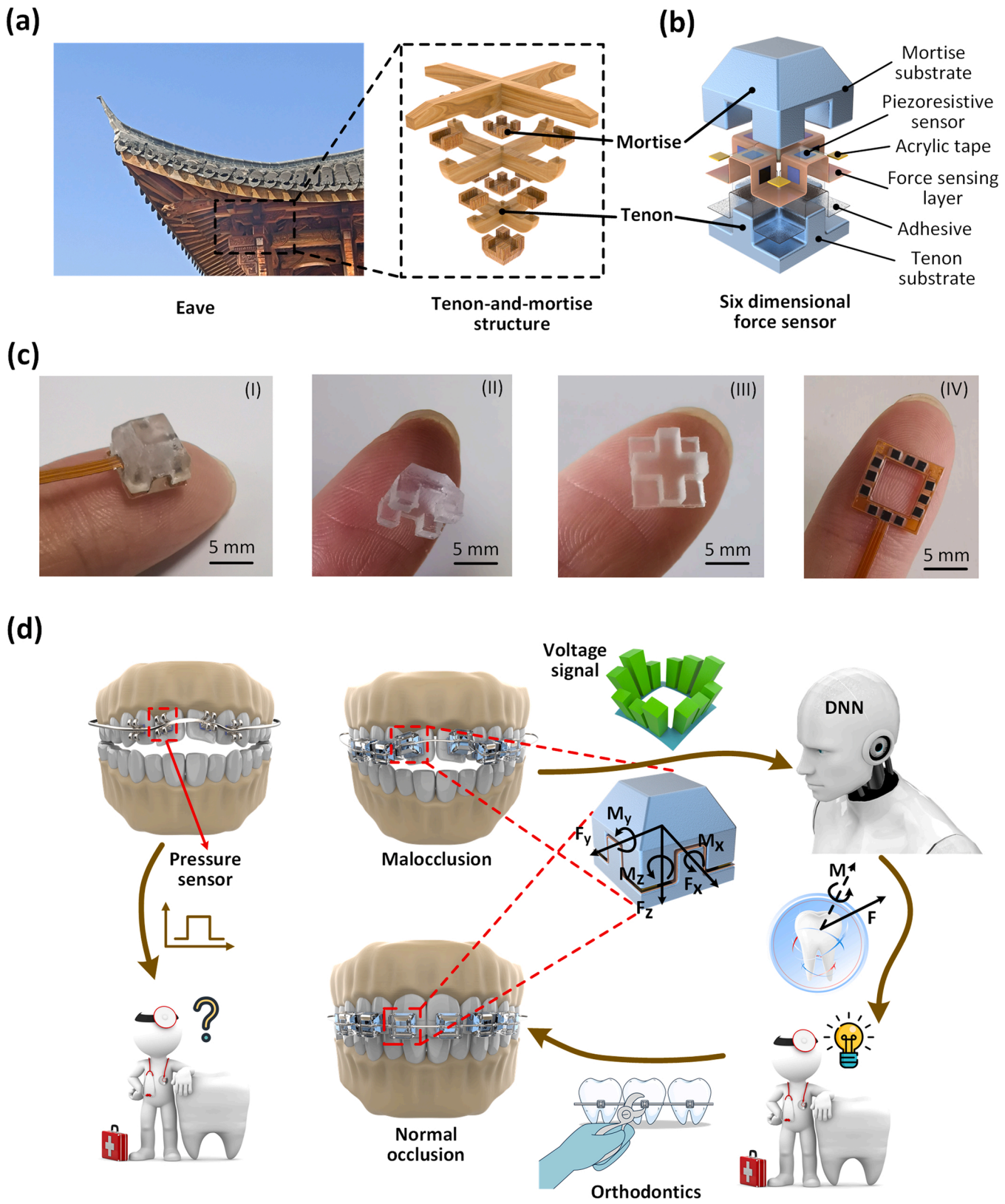

Fig. 1. Tenon and mortise structure of Chinese ancient architecture-inspired six-dimensional tactile sensor. (a) The tenon-and-mortise structure of the eaves of ancient Chinese buildings. (b) The exploded view of the six-dimensional force sensor. (c) The physical image of six-dimensional force sensor: (I) Flexible six-dimensional force sensor; (II) Mortise substrate; (III) Tenon substrate; (Ⅳ)Force sensing layer. (d) Flow chart of application of flexible six-dimensional force sensor in orthodontics compared with pressure sensor.

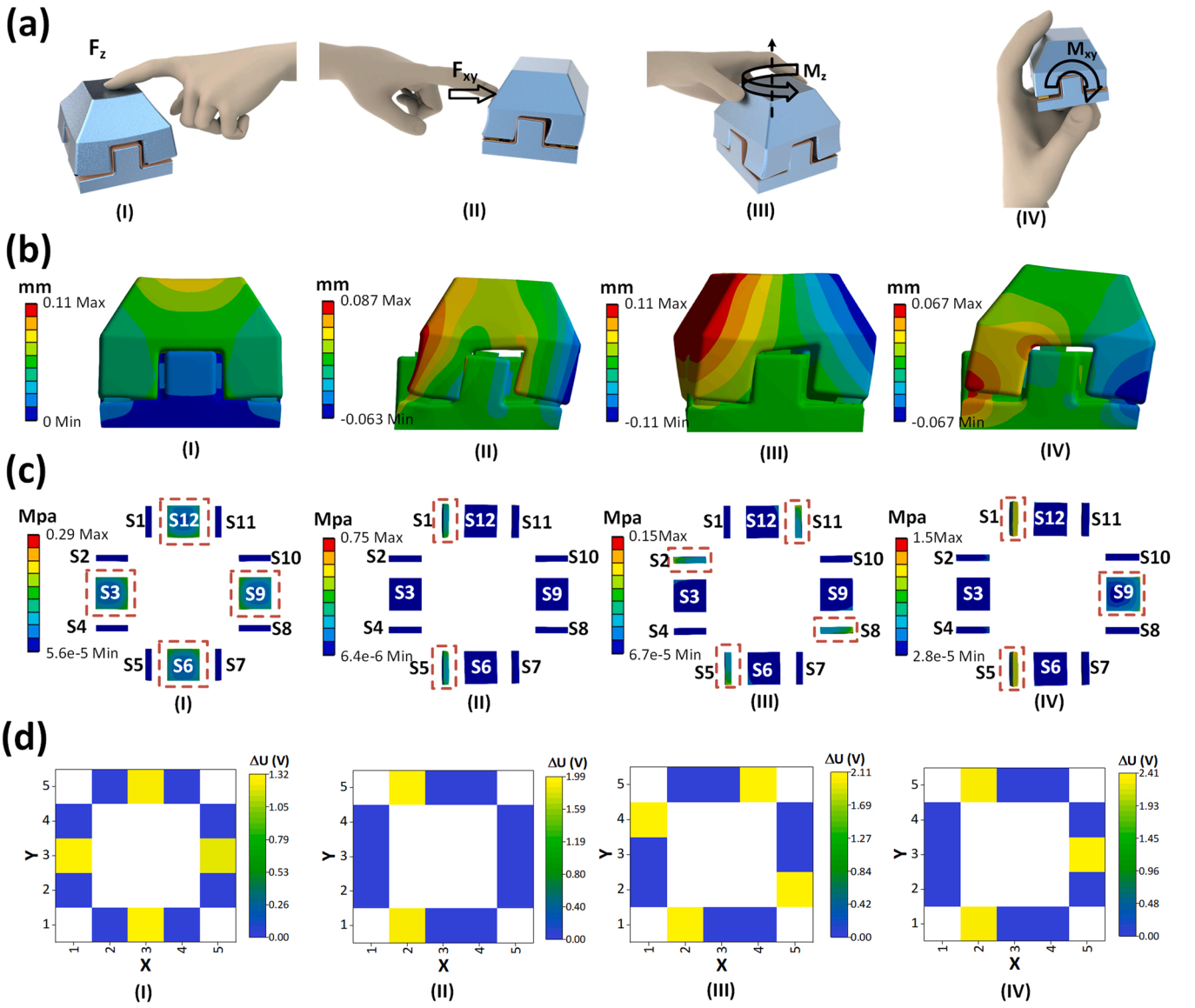

Fig. 2. The sensing mechanism of the flexible six-dimensional force sensor. (a) Schematic diagram of sensor subjected to the six-dimensional force. (b) The finite element directional deformation diagram of the sensor is subjected to six-dimensional force. (c) The sensor unit's finite element equivalent stress diagram when the sensor is subjected to the six-dimensional force. (d) The voltage signal response diagram when the sensor is subjected to the six-dimensional force.

and S9. The results show that the flexible six-dimensional force sensor can fully use the four different deformation modes of the tenon-and-mortise structure to detect complex external stimuli.

2.3. Experimental calibration of the flexible six-dimensional force sensor

To calibrate the sensor statically, we designed four loading methods to load the sensor with positive pressure, lateral force, z-axis torque, and lateral torque (Fig. 3**a**). For the convenience and accuracy of the loading operation, this work uses the mechanical testing system (INSTRON LEGEND2345) to load the pressure and uses the data collector (DAQ-VANTECH USB_HRF4028) to collect data.

The three-dimensional force calibration method is relatively simple, and the positive pressure is calibrated by direct loading. The lateral force is obtained by converting the positive pressure through the L-shaped fixture, and then the sensor is calibrated with the lateral force F_{xy}. The three-dimensional torque calibration method is more complicated. The *z*-axis torque calibration device is composed of ① mechanical testing system ② moment arm ③ bearing support (including bearing) ④ rotating shaft ⑤ connector ⑥ six-dimensional tactile sensor ⑦ support. The device converts the vertical downward pressure into torque M_z to calibrate the torque M_z of the sensor. The calibration principle of torque M_{xy} is to calibrate by generating torque through the force arm. The method is to use L-shaped support to make the force parallel to the top surface of the mortise substrate. The force arm d is the distance from the top surface of the mortise substrate to the center plane of longitudinal sensing units. Then, the torque M_{xy} acting on the sensor is obtained according to the Formula $M = Fd$.

The calibration curve of the sensor is obtained by sequentially loading six-dimensional forces on the sensor (Fig. 3e and f). According to the calibration curve of the sensor, the detection range of positive pressure F_z of the sensor is 0.1 N ~ 3 N, the detection range of lateral forces F_x and F_y are − 1 N ~ 1 N, and the detection range of torque M_z, M_x, and M_y are − 4 N·mm ~ 4 N·mm. When the detection range of force and torque exceeds 20%, the interlocking relationship between sensor substrates will be broken; meanwhile, the voltage change of the sensing unit is too small to distinguish the pressure change. Due to various factors such as hysteresis, creep, friction and clearance, and the influence of external conditions, the input and output characteristics of the sensor are nonlinear to a certain extent. After cyclically loading the

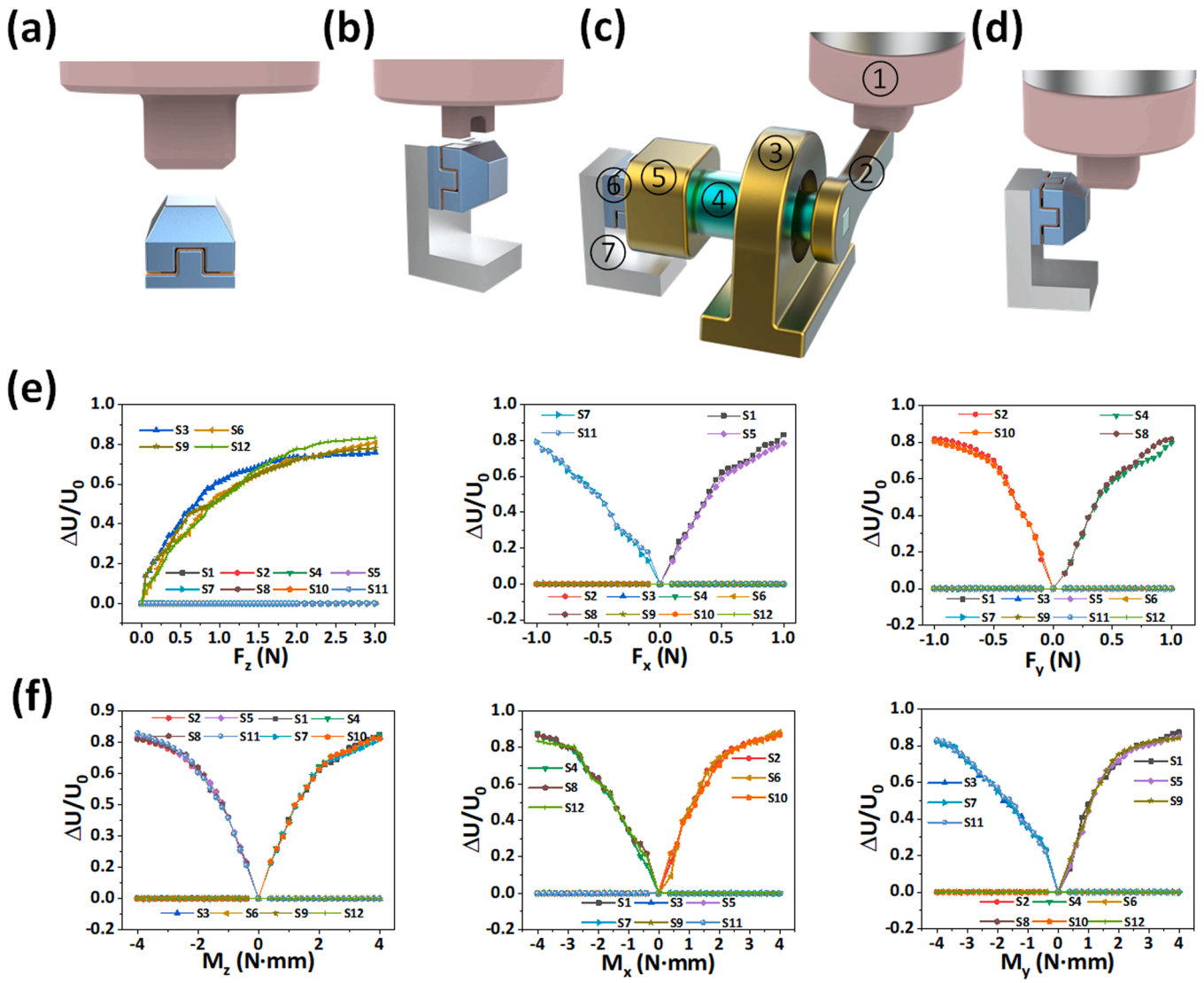

Fig. 3. Static calibration of the sensor. (a) Positive pressure loading method of the sensor. (b) Sensor's lateral force loading method. (c) Sensor's z-axis torque loading method. (d) Transverse torque loading method of the sensor. (①Mechanical testing system②Force arm③Bearing support (including bearing)④Rotating shaft⑤-Connector for connecting the shaft to the sensor⑥Six dimensional tactile sensor⑦support) (e) Sensor's three-dimensional force calibration results. (f) Sensor's three-dimensional torque calibration results.

sensor with six-dimensional forces, the sensor was found to possess good stability and repeatability (Figure. S7, S8, and S9, Supporting Information).

2.4. Theoretical calibration of sensor and DNN calibration

When the outside stimulates the six-dimensional force sensor, the voltage signals of 12 sensing units will produce a particular response. To map 12 voltage signals into six-dimensional forces, we theoretically calculate the calibration matrix *Gc* of the six-dimensional force sensor, and at the same time, obtain the linearity of the sensor (Note S2, Supporting Information). The calibration matrix of the sensor is the mapping relationship matrix between the loaded six-dimensional external force and the output voltage of the sensing unit [33]. From the linearity error matrix (Figure. S10a, Supporting Information), the measurement accuracy of each dimensional force and torque component of the sensor is as follows: F_x is 0.076, F_y is 0.107, F_z is 0.135, M_x is 0.120, M_y is 0.071, M_z is 0.067. To further improve the calibration accuracy, this work used DNN for nonlinear calibration.

The calibration process of the six-dimensional force sensor using the DNN is as follows (Fig. 4a): firstly, bias the experimental calibration data, and randomly select 60% of the data as the training sample of the DNN and 40% of the data as the test sample. Then, the column vector $S = [S_1 \quad S_2 \quad S_3 \quad S_4 \quad S_5 \quad S_6 \quad S_7 \quad S_8 \quad S_9 \quad S_{10} \quad S_{11} \quad S_{12}]^T$ composed of the voltage values output by 12 piezoresistive sensing units is constructed as the input vector of the six-dimensional tactile sensor DNN. The column vector $F_W = [F_x \quad F_y \quad F_z \quad M_x \quad M_y \quad M_z]^T$ composed of the corresponding six equal force/torque components acting on the coordinate origin of the sensor is used as the output vector of the sensor system DNN. Considering that the 12-channel voltage signal has the characteristics of nonlinearity and coupling, in the design of the hidden layer, it is necessary to expand the dimension of the 12-channel data first and then reduce the dimension, to analyze the hidden features in the input signal as much as possible. In theory, the more nodes in each layer and the more hidden layers, the higher the accuracy of the results obtained by the network. In actual applications, three hidden layers are finally retained to balance the computational complexity and the accuracy of the results. The size of the hidden layers is 96, 192, 384, and the activation function between the layers is ReLU. The root means square error (RMSE) is used to describe the output loss of the training

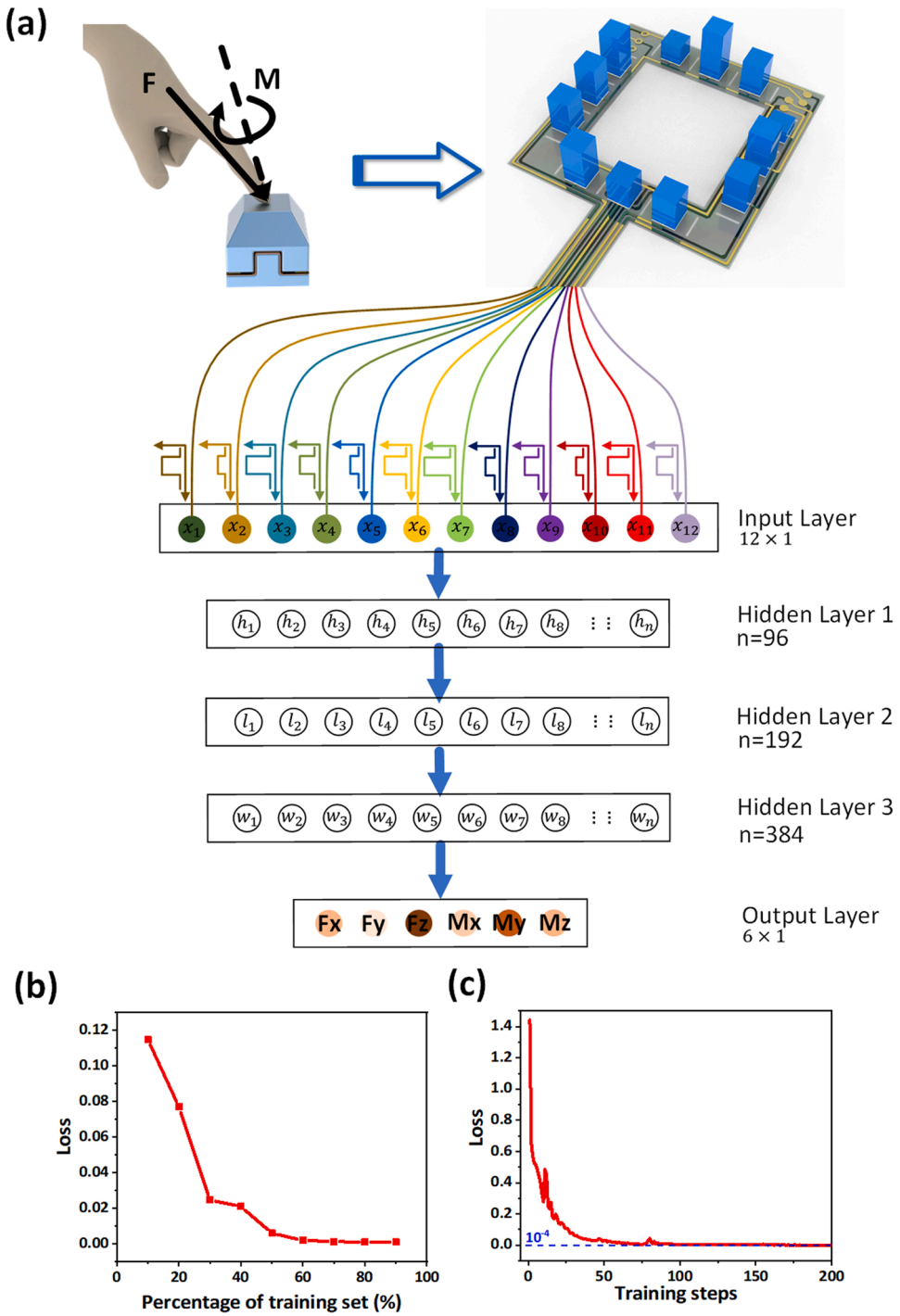

Fig. 4. DNN for the six-dimensional tactile sensor calibration. (a) DNN network framework diagram. (b) The number of training samples versus MMSE. (c) Training error curve of DNN.

sample, and the loss function is optimized by the gradient descent method. To obtain the minimum number of training samples to calibrate the sensor output, we tested the decoupling ability of DNNs with different numbers of training samples. By continuously reducing the training set sample size, the training is repeated several times and cross-validated using minimum mean square error (MMSE). The results show that DNN can learn more good mappings when the training samples are 60% or more (Fig. 4b). We finally randomly selected 60% of all experimental samples for further training to obtain higher training accuracy. When the network is trained to 200 steps, the error magnitude is reduced to 10^{-4} (Fig. 4c).

From the error matrix, the measurement accuracy of each dimensional force and torque component of the sensor is as follows: F_x is 0.042, F_y is 0.082, F_z is 0.008, M_x is 0.011, M_y is 0.012, M_z is 0.004. When F_y direction is loaded, the coupling between dimensions in M_y direction is the largest, and the maximum error is 0.012 (Figure. S10b, Supporting Information). Finally, the variation curve between the force value measured in each sensor direction and the standard load force value is obtained (Figure. S11, Supporting Information). It can be seen that after being optimized by DNN, the sensor has high linearity and low dimensional coupling and can identify the six-dimensional force with high precision.

We also evaluate the performance of the flexible six-dimensional force sensor by comparing their sensing signals with the rigid six-dimensional force sensor (Nano 17, ATI Industrial Automation, Fig. S12, Supporting Information). For a more convincing comparison, we specifically designed the compound force and moment loading platform to apply the same force and moment to both sensors (Figure. S13, Supporting Information). The compound force and moment loading platform apply three-dimensional force or three-dimensional moment by loading weights. The testing result indicates that the performance of the flexible six-dimensional force sensor was similar to that of the rigid six-dimensional force sensor under the same loading conditions (Figure. S14, Supporting Information), with an error of about 9.4%, which can meet the requirements of sensing accuracy.

2.5. Application of the six-dimensional force sensor in orthodontics

The current orthodontic treatment mainly relies on the patient's subjective perception and the dentist's treatment experience, making it difficult to acquire the orthodontic force with appropriate size and direction to further minimize the side effects [62] (e.g., root resorption, pulp inflammation, tooth pain, and loosening). Therefore, a flexible six-dimensional force sensor is essential for orthodontics (Figure. S15, Supporting Information). As a proof-of-concept demonstration, the capability of six-dimensional force sensing of the sensor is then exploited for the potential application in orthodontic treatment. Biocompatible and durable materials (e.g., PDMS [63], PI [64], and PTFE [65]) were adopted to prepare the sensor. We also demonstrated through finite element analysis that the sensor placed between the brackets and the teeth does not affect the transmission of orthodontic forces (Figure. S16, Supporting Information). Meanwhile, PDMS as the preparation material within the sensor does not affect the orthodontic results (Figure. S17, Supporting Information).

We have conducted additional experiments to evaluate further the sensor's performance in a moist environment for orthodontics application. Different orthodontic forces were applied to the bracket and sensor by adjusting the shape of the archwire to demonstrate the sensor's performance under various forces. The six-dimensional force sensing signals of the sensors were then measured in an air environment at room temperature of 25 °C. Next, one set of sensors was placed in the air at 36.5 °C, and the remaining three sets of sensors were placed in an artificial saliva reagent (AR-8802, Dongguan Kehong Chemical Co., Ltd.) at 36.5 °C to simulate a humid oral environment at 36.5 °C. The sensing signals were tested once an hour for 7 h. The results show that our flexible six-dimensional force sensor has a stable sensing capability in the artificial saliva reagent at 36.5 °C (Figure. S18, Supporting Information).

Then we explored the role of sensors in orthodontics by integrating flexible six-dimensional force sensors into 3D printed dentures (Fig. 5a). During the process of orthodontics, the deformed stainless-steel wire utilizes the release of internal stress to apply orthodontic forces on the teeth through the braces, thereby correcting the teeth from the skewed posture (green part) to the normal posture (blue region) (Fig. 5b). The response of the four sensors installed on the tooth surface to the voltage signal generated by the tooth orthodontic force, as is shown (Fig. 5c), and the mapped six-dimensional force is calculated by DNN (Fig. 5d). These six-dimensional force sensing information have unique advantages in assisting dentists to obtain the orthodontic force of braces on teeth, which can benefit the effectiveness of orthodontics treatment.

To further explore the role of the six-dimensional force sensor in real-time orthodontic treatment, we use the sensor to detect the changes of orthodontic force in the whole process of denture posture correction (Fig. 5e). In the process of denture posture correction, the six-dimensional force sensor can sense the magnitude and direction of the orthodontic force on the teeth at each stage (Fig. 5f and g). In particular, a larger torque and force are required to rotate and move the teeth in the right direction (F = 0.45 N, M = 1.9 N·mm) during the early stages of orthodontic treatment. In the mid-stage of orthodontics, the orthodontic force needs to be readjusted due to the change of the teeth position, which leads to a movement of the teeth towards the right side (F = 0.26 N, M = 1.55 N·mm). In the final stage of orthodontics, a certain amount of orthodontic force is necessary to be applied to maintain the teeth in the same position (F = 0.15 N, M = 0.77 N·mm). Thus, these six-dimensional force sensing information can assist dentists in checking whether the orthodontic force is appropriate and whether the braces are loose to timely adjust the deformation of the stainless-steel wire.

3. Conclusions

In conclusion, this work uses the tenon-and-mortise structure of ancient Chinese buildings for reference to design a flexible sensor that can quantitatively detect six-dimensional force, achieving a breakthrough in the direction of the flexible sensor for six-dimensional force perception (Table S1, Supporting Information). Here, when the sensor is subjected to a six-dimensional force, the four different deformation mechanisms will cause the 12 sensing units to generate corresponding unique voltage signals. The signal response of the sensor under the six-dimensional force is obtained through the calibration experiment. Then the calibration matrix G_c of the sensor is obtained after theoretical calculation, and the average linear error does not exceed 0.082. We also use DNN to optimize the calibration accuracy further and reduce the average linearity error to 0.008. Meanwhile, the sensor has a wide detection range (F_x 0.1 N ~ 3 N, F_y −1 N ~ 1 N, F_z −1 N ~ 1 N, M_x −4 N·mm ~ 4 N·mm, M_y −4 N·mm ~ 4 N·mm, M_z −4 N·mm ~ 4 N·mm). In orthodontics, the six-dimensional force sensor can effectively detect the orthodontic force's magnitude and direction on the teeth and guide the dentists to conduct targeted orthodontics. We believe that our research can provide new ideas for the development of multi-dimensional tactile sensors. These multi-dimensional tactile sensors can have various medical diagnosis tools and human health detection systems to help robots perceive more dimensional force information.

4. Experimental section

Preparation of the six-dimensional force sensor (Fig. S9, Supporting Information). Firstly, we prepared the mold of mortise and tenon base through the 3D printer (Form 2, Formlabs), then configured PDMS (Sylgard 184, Dow Corning) in the ratio of 5:1, vacuumed the PDMS, poured it into the mold, heated at 80 ℃ for one hour. Then we got the tenon-and-mortise base of the sensor after demolding. Next, cut the pressure-sensitive conductive sheet (Sichiray) into 12 pieces 1 × 1 mm^2 square. The pressure-sensitive conductive sheet is encapsulated on the FPCB through PTFE to obtain the force sensing layer. Then, we pasted the force sensing layer folded along the small hole (0.1 mm × 1 mm) to the tenon substrate through adhesive. Finally, we pasted the four feet of the mortise substrate with the force sensing layer by acrylic type to obtain the six-dimensional tactile sensor.

Computational platform for the DNN model. This work uses the Python language and the Pytorch deep learning framework to build the DNN model, and due to the small size of the designed DNN, the experiments can be trained using the CPU.

CRediT authorship contribution statement

Jiahui Hu: Writing – original draft, Data curation, Validation. **Ye Qiu:** Formal analysis, Validation. **Xueer Wang:** Investigation. **Lelun Jiang:** Validation. **Xiaoyan Lu:** Validation. **Ming Li:** Validation. **Zhiqiang Wang:** Data curation, Validation. **Kai Pang:** Project administration. **Ye Tian:** Writing – review & editing. **Wenan Zhang:** Writing – review & editing. **Zhen Xu:** Data curation, Validation. **Hengjie Zhang:** Data curation, Validation. **Hangcheng Qi:** Data curation, Validation. **Aiping Liu:** Project administration. **Zheng Zhang:** Project

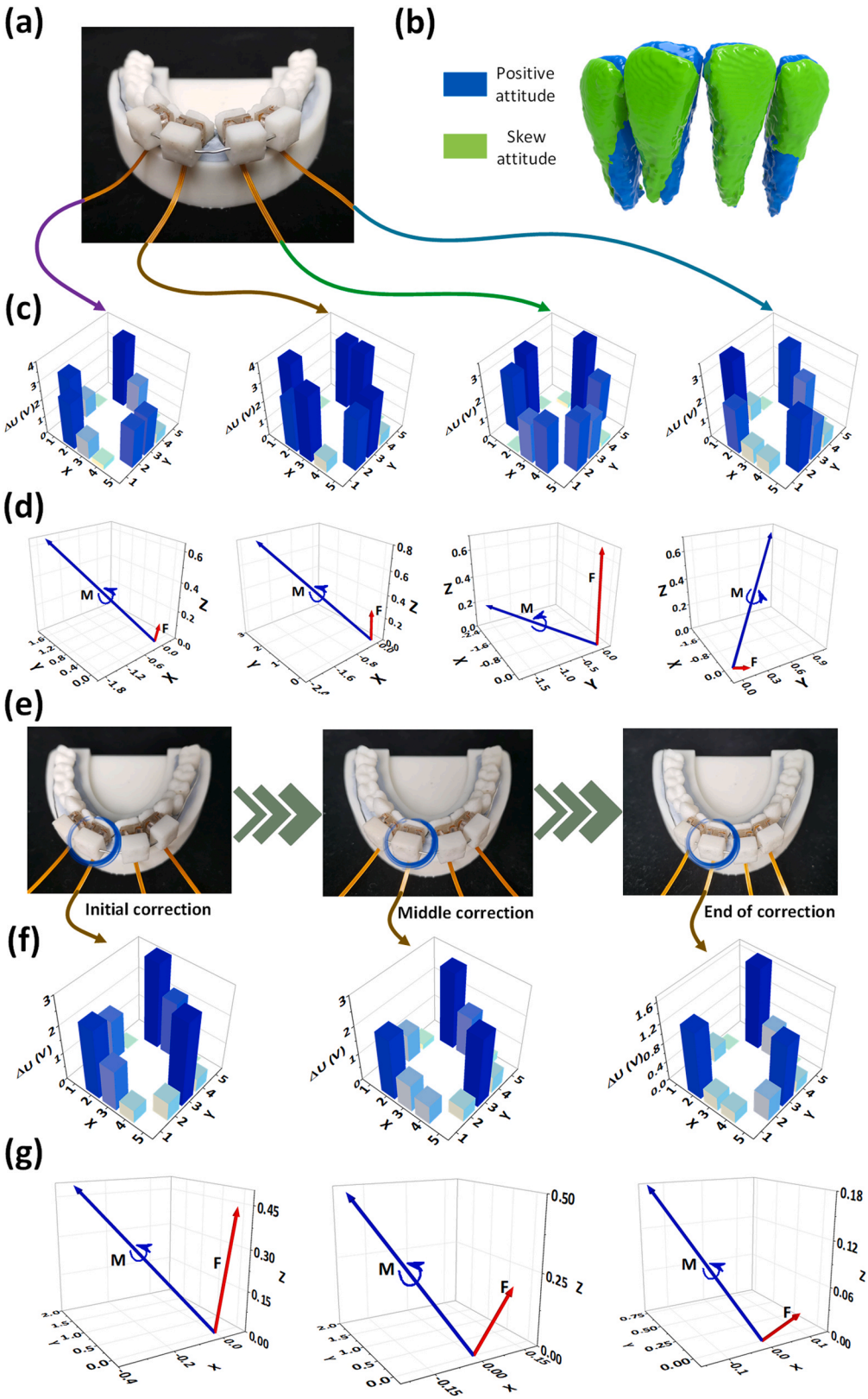

Fig. 5. Application of the six-dimensional tactile sensor in orthodontics. (a) Schematic diagram of the six-dimensional tactile sensor installed on the denture. (b) Schematic diagram of correction of the crooked denture to normal posture. (c) Voltage signal diagram of four six-dimensional tactile sensors subjected to orthodontic force. (d) The six-dimensional force obtained after the sensor voltage signal is calculated by the DNN neural network. (e) Schematic diagram of left lower front teeth in three stages: initial correction, middle correction, and end of correction. (f) Voltage signal response diagram of the six-dimensional tactile sensor installed on the left lower incisor in three stages. (g) The six-dimensional force is obtained by calculating the DNN neural network of the sensor voltage signal in the three correction stages.

administration. **Huaping Wu:** Writing – review & editing, Project administration.

Declaration of Competing Interest

The authors declare that they have no known competing financial interests or personal relationships that could have appeared to influence the work reported in this paper.

Acknowledgments

This work was supported by National Natural Science Foundation of China (Grant no. 11972323, 11672269, 51675485, 51572242 and 12002308); Zhejiang Provincial Natural Science Foundation of China (Grant no. LQ22A020009, LR20A020002, LR18E050002, LR19E020004, LZY21E030002, and D21F030003); Fundamental Research Funds for the Provincial Universities of Zhejiang (RF-B2019004); 111 Project (No.: D16004); Department of Education of Zhejiang Province (Y202043208).

Appendix A. Supporting information

Supplementary data associated with this article can be found in the online version at doi:10.1016/j.nanoen.2022.107073.

References

[1] D.B. Chen, Q.P. Liu, Z.W. Han, J.Q. Zhang, H.L. Song, K.J. Wang, Z.Y. Song, S. F. Wen, Y. Zhou, C.Z. Yan, Y.S. Shi, 4D printing strain self-sensing and temperature self-sensing integrated sensor-actuator with bioinspired gradient gaps, Adv. Sci. 7 (2020), 2000584, https://doi.org/10.1002/advs.202000584.

[2] Y.H. Jung, J.H. Kim, J.A. Rogers, Skin-integrated vibrohaptic interfaces for virtual and augmented reality, Adv. Funct. Mater. 31 (2021), 2008805, https://doi.org/10.1002/adfm.202008805.

[3] Y. Qiu, C.J. Wang, X.Y. Lu, H.P. Wu, X.L. Ma, J.H. Hu, H.C. Qi, Y. Tian, Z. Zhang, G. J. Bao, H. Chai, J.Z. Song, A.P. Liu, A biomimetic drosera capensis with adaptive decision-predation behavior based on multifunctional sensing and fast actuating capability, Adv. Funct. Mater. (2021), 2110296, https://doi.org/10.1002/adfm.202110296.

[4] S. Sundaram, P. Kellnhofer, Y.Z. Li, J.Y. Zhu, A. Torralba, W. Matusik, Learning the signatures of the human grasp using a scalable tactile glove, Nature 569 (2019) 698, https://doi.org/10.1038/s41586-019-1234-z.

[5] T.T. Yang, D. Xie, Z.H. Li, H.W. Zhu, Recent advances in wearable tactile sensors: materials, sensing mechanisms, and device performance, Mater. Sci. Eng. R. Rep. 115 (2017) 1–37, https://doi.org/10.1016/j.mser.2017.02.001.

[6] Z.R. Zhai, Y. Wang, K. Lin, L.L. Wu, H.Q. Jiang, In situ stiffness manipulation using elegant curved origami, Sci. Adv. 6 (2020) eabe2000, https://doi.org/10.1126/sciadv.abe2000.

[7] W. Ling, G. Liew, Y. Li, Y.F. Hao, H.Z. Pan, H.J. Wang, B.A. Ning, H. Xu, X. Huang, Materials and techniques for implantable nutrient sensing using flexible sensors integrated with metal-organic frameworks, Adv. Mater. 30 (2018), 1800917, https://doi.org/10.1002/adma.201800917.

[8] H. Yang, M. Wang, M. Deng, H. Guo, W. Zhang, H. Yang, Y. Xi, X. Li, C. Hu, Z. Wang, A full-packaged rolling triboelectric-electromagnetic hybrid nanogenerator for energy harvesting and building up self-powered wireless systems, Nano Energy 56 (2019) 300–306, https://doi.org/10.1016/j.nanoen.2018.11.043.

[9] Y. Du, Q. Tang, W. He, W. Liu, Z. Wang, H. Wu, G. Li, H. Guo, Z. Li, Y. Peng, C. Hu, Harvesting ambient mechanical energy by multiple mode triboelectric nanogenerator with charge excitation for self-powered freight train monitoring, Nano Energy 90 (2021), 106543, https://doi.org/10.1016/j.nanoen.2021.106543.

[10] Q. Xu, J. Wen, Y. Qin, Development and outlook of high output piezoelectric nanogenerators, Nano Energy 86 (2021), 106080, https://doi.org/10.1016/j.nanoen.2021.106080.

[11] N. Sezer, M. Koç, A comprehensive review on the state-of-the-art of piezoelectric energy harvesting, Nano Energy 80 (2021), 105567, https://doi.org/10.1016/j.nanoen.2020.105567.

[12] W. Yan, H.-R. Fuh, Y. Lv, K.-Q. Chen, T.-Y. Tsai, Y.-R. Wu, T.-H. Shieh, K.-M. Hung, J. Li, D. Zhang, C.Ó. Coileáin, S.K. Arora, Z. Wang, Z. Jiang, C.-R. Chang, H.-C. Wu, Giant gauge factor of Van der Waals material based strain sensors, Nat. Commun. 12 (2021) 2018, https://doi.org/10.1038/s41467-021-22316-8.

[13] F. Yi, X. Wang, S. Niu, S. Li, Y. Yin, K. Dai, G. Zhang, L. Lin, Z. Wen, H. Guo, J. Wang, M.-H. Yeh, Y. Zi, Q. Liao, Z. You, Y. Zhang, L. Wang Zhong, A highly shape-adaptive, stretchable design based on conductive liquid for energy harvesting and self-powered biomechanical monitoring, Sci. Adv. 2 (2016), e1501624, https://doi.org/10.1126/sciadv.1501624.

[14] Z.Y. Gao, K. Jiang, Z. Lou, W. Han, G.Z. Shen, Water-proof and thermally inert flexible pressure sensors based on zero temperature coefficient of resistance hybrid films, J. Mater. Chem. C 7 (2019) 9648–9654, https://doi.org/10.1039/c9tc02832c.

[15] Y. Qiu, Y. Tian, S.S. Sun, J.H. Hu, Y.Y. Wang, Z. Zhang, A.P. Liu, H.Y. Cheng, W. Z. Gao, W.N. Zhang, H. Chai, H.P. Wu, Bioinspired, multifunctional dual -mode pressure sensors as electronic skin for decoding complex loading processes and human motions, Nano Energy 78 (2020), 105337, https://doi.org/10.1016/j.nanoen.2020.105337.

[16] Y.Q. Song, W.T. Huang, C.H. Mu, X.X. Chen, Q.H. Zhang, A. Ran, Z.R. Peng, R. J. Sun, W.H. Xie, Carbon nanotube-modified fabric for wearable smart electronic-skin with exclusive normal-tangential force sensing ability, Adv. Mater. Technol. 4 (2019), 1800680, https://doi.org/10.1002/admt.201800680.

[17] J. Zhang, L.J. Zhou, H.M. Zhang, Z.X. Zhao, S.L. Dong, S. Wei, J. Zhao, Z.L. Wang, B. Guo, P.A. Hu, Highly sensitive flexible three-axis tactile sensors based on the interface contact resistance of microstructured graphene, Nanoscale 10 (2018) 7387–7395, https://doi.org/10.1039/c7nr09149d.

[18] L. Viry, A. Levi, M. Totaro, A. Mondini, V. Mattoli, B. Mazzolai, L. Beccai, Flexible three-axial force sensor for soft and highly sensitive artificial touch, Adv. Mater. 26 (2014) 2659–2664, https://doi.org/10.1002/adma.201305064.

[19] W.L. Liu, Z. Wang, G. Wang, G.L. Liu, J. Chen, X.J. Pu, Y. Xi, X. Wang, H.Y. Guo, C. G. Hu, Z.L. Wang, Integrated charge excitation triboelectric nanogenerator, Nat. Commun. 10 (2019) 1426, https://doi.org/10.1038/s41467-019-09464-8.

[20] M.D. Han, H.L. Wang, Y.Y. Yang, C.M. Liang, W.B. Bai, Z. Yan, H.B. Li, Y.G. Xue, X. L. Wang, B. Akar, H.B. Zhao, H.W. Luan, J. Lim, I. Kandela, G.A. Ameer, Y. H. Zhang, Y.G. Huang, J.A. Rogers, Three-dimensional piezoelectric polymer microsystems for vibrational energy harvesting, robotic interfaces and biomedical implants, Nat. Electron. 2 (2019) 26–35, https://doi.org/10.1038/s41928-018-0189-7.

[21] Y. Qiu, S.S. Sun, C. Xu, Y.Y. Wang, Y. Tian, A.P. Liu, X. Hou, H. Chai, Z. Zhang, H. P. Wu, The frequency-response behaviour of flexible piezoelectric devices for detecting the magnitude and loading rate of stimuli, J. Mater. Chem. C 9 (2021) 584–594, https://doi.org/10.1039/d0tc02949a.

[22] S. Wang Hee, K. Hong Seong, H. Han Jae, H. Jung Young, K. Jeong Hyun, H. Im Tae, K. Jeong Chang, B.-Y. Lee, G. Kim, D. Yoo Chang, J. Lee Keon, Biomimetic and flexible piezoelectric mobile acoustic sensors with multiresonant ultrathin structures for machine learning biometrics, Sci. Adv. 7 (2021) eabe5683, https://doi.org/10.1126/sciadv.abe5683.

[23] D. Maurya, S. Khaleghian, R. Sriramdas, P. Kumar, R.A. Kishore, M.G. Kang, V. Kumar, H.-C. Song, S.-Y. Lee, Y. Yan, J.-M. Park, S. Taheri, S. Priya, 3D printed graphene-based self-powered strain sensors for smart tires in autonomous vehicles, Nat. Commun. 11 (2020) 5392, https://doi.org/10.1038/s41467-020-19088-y.

[24] K. Sun, H. Ko, H.H. Park, M. Seong, S.H. Lee, H. Yi, H.W. Park, T.I. Kim, C. Pang, H. E. Jeong, Hybrid Architectures of Heterogeneous Carbon Nanotube Composite Microstructures Enable Multiaxial Strain Perception with High Sensitivity and Ultrabroad Sensing Range (vol 14, 1803411, 2018), Small 15 (2019), 1900161, https://doi.org/10.1002/smll.201900161.

[25] J. Yang, S. Luo, X. Zhou, J.L. Li, J.T. Fu, W.D. Yang, D.P. Wei, Flexible, tunable, and ultrasensitive capacitive pressure sensor with microconformal graphene electrodes, ACS Appl. Mater. Interfaces 11 (2019) 14997–15006, https://doi.org/10.1021/acsami.9b02049.

[26] B.Q. Nie, R.Y. Li, J.D. Brandt, T.R. Pan, Microfluidic tactile sensors for three-dimensional contact force measurements, Lab Chip 14 (2014) 4344–4353, https://doi.org/10.1039/c4lc00746h.

[27] H. Oh, G.C. Yi, M. Yip, S.A. Dayeh, Scalable tactile sensor arrays on flexible substrates with high spatiotemporal resolution enabling slip and grip for closed-loop robotics, Sci. Adv. 6 (2020) eabd7795, https://doi.org/10.1126/sciadv.abd7795.

[28] B. Park, Y. Lee, W. Jung, D.K. Scott, D. Aalto, H.J. Chung, T.I. Kim, Deterministically assigned directional sensing of a nanoscale crack based pressure sensor by anisotropic Poisson ratios of the substrate dagger, J. Mater. Chem. C 9 (2021) 5154–5161, https://doi.org/10.1039/d1tc00416f.

[29] M. Wu, J.S. Chen, Y.H. Ma, B. Yan, M.F. Pan, Q.Y. Peng, W.D. Wang, L.B. Han, J. F. Liu, H.B. Zeng, Ultra elastic, stretchable, self-healing conductive hydrogels with tunable optical properties for highly sensitive soft electronic sensors, J. Mater. Chem. A 8 (2020) 24718–24733, https://doi.org/10.1039/d0ta09735g.

[30] C. Zhang, H.X. Zheng, J. Sun, Y.S. Zhou, W.H. Xu, Y.H. Dai, J.Y. Mo, Z.A.K. Wang, 3D printed, solid-state conductive ionoelastomer as a generic building block for tactile applications, Adv. Mater. (2021), 2105996, https://doi.org/10.1002/adma.202105996.

[31] P.C. Zhu, C.Q. Shi, Y.L. Wang, Y.L. Wang, Y.D. Yu, Y. Wang, Y. Deng, J.L. Xiao, Recyclable, healable, and stretchable high-power thermoelectric generator, Adv. Energy Mater. 11 (2021), 2100920, https://doi.org/10.1002/aenm.202100920.

[32] W. Ke, D. Fuzhou, Z. Jiabo, Y. JiZhi, An alignment method of human-robot collaboration based on the six-dimensional force/torque dynamic measurement for large-scale components, J. Robot. 2018 (2018), 2914871, https://doi.org/10.1155/2018/2914871.

[33] Y.J. Li, C. Yang, G.C. Wang, H. Zhang, H.Y. Cui, Y.L. Zhang, Research on the parallel load sharing principle of a novel self-decoupled piezoelectric six-dimensional force sensor, ISA Trans. 70 (2017) 447–457, https://doi.org/10.1016/j.isatra.2017.07.008.

[34] W. Liu, Y.J. Li, Z.Y. Jia, J. Zhang, M. Qian, Research on parallel load sharing principle of piezoelectric six-dimensional heavy force/torque sensor, Mech. Syst. Signal Process 25 (2011) 331–343, https://doi.org/10.1016/j.ymssp.2010.09.008.

[35] Z. Tong, H. Jiang, J. He, H. Zhang, Optimal Design of the Isotropy Performance of a Six-dimensional Force Sensor Based on a Generalized Gough-Stewart Structure Lying on a Pair of Circular Hyperboloids, Acta Aeronaut. Astronaut. Sin. (China) 34 (2013) 177–185, https://doi.org/10.7527/s1000-6893.2013.0165.

[36] F. Zeng, J.L. Xiao, H.T. Liu, Force/Torque Sensorless Compliant Control Strategy for Assembly Tasks Using a 6-DOF Collaborative Robot, Ieee Access 7 (2019) 108795–108805, https://doi.org/10.1109/access.2019.2931515.
[37] Z.J. Zhang, Y.P. Chen, D.L. Zhang, J.M. Xie, M.Y. Liu, A six-dimensional traction force sensor used for human-robot collaboration, Mechatronics 57 (2019) 164–172, https://doi.org/10.1016/j.mechatronics.2018.12.005.
[38] D. Choi, S. Jang, J.S. Kim, H.J. Kim, D.H. Kim, J.Y. Kwon, A Highly sensitive tactile sensor using a pyramid-plug structure for detecting pressure, shear force, and torsion, Adv. Mater. Technol. 4 (2019), 1800284, https://doi.org/10.1002/admt.201800284.
[39] S.M. Won, H. Wang, B.H. Kim, K. Lee, H. Jang, K. Kwon, M. Han, K.E. Crawford, H. Li, Y. Lee, X. Yuan, S.B. Kim, Y.S. Oh, W.J. Jang, J.Y. Lee, S. Han, J. Kim, X. Wang, Z. Xie, Y. Zhang, Y. Huang, J.A. Rogers, Multimodal sensing with a three-dimensional piezoresistive structure, Acs Nano 13 (2019) 10972–10979, https://doi.org/10.1021/acsnano.9b02030.
[40] I. You, D.G. Mackanic, N. Matsuhisa, J. Kang, J. Kwon, L. Beker, J. Mun, W. Suh, T. Y. Kim, J.B.H. Tok, Z.N. Bao, U. Jeong, Artificial multimodal receptors based on ion relaxation dynamics, Science 370 (2020) 961, https://doi.org/10.1126/science.aba5132.
[41] F. Zhang, P.C. Ma, J.X. Wang, Q. Zhang, W. Feng, Y.W. Zhu, Q.B. Zheng, Anisotropic conductive networks for multi-dimensional sensing, Mater. Horiz. 8 (2021) 2615–2653, https://doi.org/10.1039/d1mh00615k.
[42] X. Zeng, Y. Liu, F. Liu, W. Wang, X. Liu, X. Wei, Y. Hu, A bioinspired three-dimensional integrated e-skin for multiple mechanical stimuli recognition, Nano Energy 92 (2022), 106777, https://doi.org/10.1016/j.nanoen.2021.106777.
[43] L. Cheng, W. Qian, L. Wei, H.J. Zhang, T.Y. Zhao, M. Li, A.P. Liu, H.P. Wu, A highly sensitive piezoresistive sensor with interlocked graphene microarrays for meticulous monitoring of human motions, J. Mater. Chem. C 8 (2020) 11525–11531, https://doi.org/10.1039/d0tc02539a.
[44] C. Pang, G.-Y. Lee, T.-I. Kim, S.M. Kim, H.N. Kim, S.-H. Ahn, K.-Y. Suh, A flexible and highly sensitive strain-gauge sensor using reversible interlocking of nanofibres, Nat. Mater. 11 (2012) 795–801, https://doi.org/10.1038/nmat3380.
[45] M.S. Suen, Y.C. Lin, R.S. Chen, A flexible multifunctional tactile sensor using interlocked zinc oxide nanorod arrays for artificial electronic skin, Sens. Actuator A Phys. 269 (2018) 574–584, https://doi.org/10.1016/j.sna.2017.11.053.
[46] C.M. Boutry, M. Negre, M. Jorda, O. Vardoulis, A. Chortos, O. Khatib, Z.N. Bao, A hierarchically patterned, bioinspired e-skin able to detect the direction of applied pressure for robotics, Sci. Robot. 3 (2018) eaau6914, https://doi.org/10.1126/scirobotics.aau6914.
[47] L. Bradley, G. Larsen, Y.P. Zhao, Designed to fail: flexible, anisotropic silver nanorod sheets for low-cost wireless activity monitoring, J. Phys. Chem. C. 120 (2016) 14969–14976, https://doi.org/10.1021/acs.jpcc.6b04792.
[48] H.M. Chen, Y. Jing, J.H. Lee, D. Liu, J. Kim, S.S. Chen, K. Huang, X. Shen, Q. B. Zheng, J.L. Yang, S. Jeon, J.K. Kim, Human skin-inspired integrated multi-dimensional sensors based on highly anisotropic structures, Mater. Horiz. 7 (2020) 2378–2389, https://doi.org/10.1039/d0mh00922a.
[49] S. Chen, Y.J. Song, D.Y. Ding, Z. Ling, F. Xu, Flexible and anisotropic strain sensor based on carbonized crepe paper with aligned cellulose fibers, Adv. Funct. Mater. 28 (2018), 1802547, https://doi.org/10.1002/adfm.201802547.
[50] S. Gao, X.Y. Wu, H.B. Ma, J. Robertson, A. Nathan, Ultrathin multifunctional graphene-PVDF layers for multidimensional touch interactivity for flexible displays, ACS Appl. Mater. Interfaces 9 (2017) 18410–18416, https://doi.org/10.1021/acsami.7b03437.
[51] K.K. Kim, S. Hong, H.M. Cho, J. Lee, Y.D. Suh, J. Ham, S.H. Ko, Highly sensitive and stretchable multi-dimensional strain sensor with prestrained anisotropic metal nanowire percolation networks, Nano Lett. 15 (2015) 5240–5247, https://doi.org/10.1021/acs.nanolett.5b01505.
[52] J.H. Lee, J.S. Heo, Y.J. Kim, J. Eom, H.J. Jung, J.W. Kim, I. Kim, H.H. Park, H. S. Mo, Y.H. Kim, S.K. Park, A behavior-learned cross-reactive sensor matrix for intelligent skin perception, Adv. Mater. 32 (2020), 2000969, https://doi.org/10.1002/adma.202000969.
[53] W.S. Lee, D. Kim, B. Park, H. Joh, H.K. Woo, Y.K. Hong, T.I. Kim, D.H. Ha, S.J. Oh, Multiaxial and transparent strain sensors based on synergetically reinforced and orthogonally cracked hetero-nanocrystal solids, Adv. Funct. Mater. 29 (2019), 1806714, https://doi.org/10.1002/adfm.201806714.
[54] G.J. Zhu, P.G. Ren, J. Hu, J.J. Yang, Y.P. Jia, Z.Y. Chen, F. Ren, J.F. Gao, Flexible and anisotropic strain sensors with the asymmetrical cross-conducting network for versatile bio-mechanical signal recognition, ACS Appl. Mater. Interfaces 13 (2021) 44925–44934, https://doi.org/10.1021/acsami.1c13079.
[55] S.Y. Chen, C. Bai, C.Y. Zhang, D. Geng, R.L. Liu, Y. Xie, W. Zhou, Flexible piezoresistive three-dimensional force sensor based on interlocked structures, Sens. Actuator A Phys. 330 (2021), 112857, https://doi.org/10.1016/j.sna.2021.112857.
[56] X. Chen, J. Shao, H. Tian, X. Li, Y. Tian, C. Wang, Flexible three-axial tactile sensors with microstructure-enhanced piezoelectric effect and specially-arranged piezoelectric arrays, Smart Mater. Struct. 27 (2018), 025018, https://doi.org/10.1088/1361-665X/aaa622.
[57] X.Y. Cheng, Y. Gong, Y.S. Liu, Z.Y. Wu, X.D. Hu, Flexible tactile sensors for dynamic triaxial force measurement based on piezoelectric elastomer, Smart Mater. Struct. 29 (2020), 075007, https://doi.org/10.1088/1361-665X/ab8748.
[58] S. Harada, K. Kanao, Y. Yamamoto, T. Arie, S. Akita, K. Takei, Fully printed flexible fingerprint-like three-axis tactile and slip force and temperature sensors for artificial skin, ACS Nano 8 (2014) 12851–12857, https://doi.org/10.1021/nn506293y.
[59] Z.Y. Liu, D.P. Qi, W.R. Leow, J.C. Yu, M. Xiloyannnis, L. Cappello, Y.Q. Liu, B. W. Zhu, Y. Jiang, G. Chen, L. Masia, B. Liedberg, X.D. Chen, 3D-structured stretchable strain sensors for out-of-plane force detection, Adv. Mater. 30 (2018), 1707285, https://doi.org/10.1002/adma.201707285.
[60] X.G. Sun, J.H. Sun, T. Li, S.K. Zheng, C.K. Wang, W.S. Tan, J.G. Zhang, C. Liu, T. J. Ma, Z.M. Qi, C.X. Liu, N. Xue, Flexible tactile electronic skin sensor with 3D force detection based on porous CNTs/PDMS nanocomposites, Nanomicro Lett. 11 (2019) 57, https://doi.org/10.1007/s40820-019-0288-7.
[61] J.Y. Yang, X.P. Li, X.Z. Lu, W.M. Bao, R.J. Chen, Three-dimensional interfacial stress sensor based on graphene foam, IEEE Sens. J. 18 (2018) 7956–7963, https://doi.org/10.1109/jsen.2018.2855691.
[62] W. Lin, M. Farella, J.S. Antoun, R.K. Topless, T.R. Merriman, A. Michelotti, Factors associated with orthodontic pain, J. Oral. Rehabil. 48 (2021) 1135–1143, https://doi.org/10.1111/joor.13227.
[63] M. Amerian, M. Amerian, M. Sameti, E. Seyedjafari, Improvement of PDMS surface biocompatibility is limited by the duration of oxygen plasma treatment, J. Biomed. Mater. Res. A 107 (2019) 2806–2813, https://doi.org/10.1002/jbm.a.36783.
[64] X.Y. Wang, J.W. Gao, J. Zhang, Biocompatibility of polyimide fibers with human gastric cells in vitro, Fibers Polym. 22 (2021) 2380–2387, https://doi.org/10.1007/s12221-021-0199-3.
[65] I. Kolesnik, T. Tverdokhlebova, N. Danilenko, E. Plotnikov, D. Kulbakin, A. Zheravin, V. Bouznik, E. Bolbasov, Characterization and determination of the biocompatibility of porous polytetrafluoroethylene membranes fabricated via electrospinning, J. Fluor. Chem. 246 (2021), 109798, https://doi.org/10.1016/j.jfluchem.2021.109798.

Jiahui Hu received his B. S. degree in Zhejiang Sci-Tech University in 2018. He is now studying for M. S. in Zhejiang University of Technology. His research interests involve solving multidimensional force perception problems in flexible tactile sensors using mechanical structure design.

Dr. Ye Qiu received her Ph. D. degree from Zhejiang University of Technology in 2021. She is currently a postdoctoral research fellow at Zhejiang University of Technology. She worked as a visiting scholar in Department of Mechanical Engineering at University of Colorado Boulder from 2018 to 2019. Her research interests include flexible electronics and smart materials/structures.

Xueer Wang received the B. S. degree from the College of Information Engineering, Zhejiang University of Technology, Hangzhou, China, in 2020, where she is currently pursuing the master's degree in control science and engineering. Her current research interests include information fusion and pattern recognition.

Lelun Jiang received the B. S. and Ph. D. degrees in mechanical engineering from South China University of Technology, Guangzhou, China in 2006 and 2011, respectively. He is currently an associate professor at School of Biomedical Engineering, Sun Yat-Sen University. His research interests focus primarily on the fabrication of biomedical devices. He has been awarded the Distinguished Young Scholars of Guangdong Science Foundation, Tip-top Scientific and Technical Innovative Youth Talents of Guangdong special support program, and the Pearl River S&T Nova Program of Guangzhou.

Xiaoyan Lu is a full professor in Harbin Institute of Technology (China). She received her Ph. D. degree from Harbin Institute of Technology in 2009. Then became an adjunct research scholar in the Pennsylvania State University from 2011 to 2012, and University of California, Berkeley, from 2015 to 2016. Her research interests include the Landau theory of ferroelectrics, domain engineering of relaxor ferroelectrics, and emergent phenomena in complex ferroelectric systems.

Dr. Ming Li received his Ph. D. degree in 2012 and became an associate professor at Dalian University of Technology. His research interests focus on the ultrathin membrane, wrinkling formation and elimination, fabrication and design of ultrathin flexible electronics.

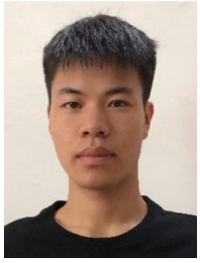

Zhiqiang Wang graduated from the School of Energy and Mechanical Engineering, Jiangxi University of Science and Technology in 2020, with a degree in engineering, and is now a master student in the School of Mechanical Engineering, Zhejiang University of Technology. His current research interests include flexible electronics and smart materials.

Dr. Kai Pang received his Ph. D. degree from Zhejiang University in 2021. He is currently a postdoctoral research fellow at Zhejiang University. His research interests include graphene macroscopic assemblies and flexible electronics.

Dr. Ye Tian is an Assistant Professor in the College of Mechanical Engineering at Zhejiang University of Technology. She received her Ph. D. degree in Materials Science from Harbin Institute of Technology in 2015. She worked as a visiting scholar in the Department of Chemical & Biomolecular Engineering at University of California, Berkeley from 2012 to 2014 and a postdoctoral research fellow in the Department of Polymer Science and Engineering at Zhejiang University from 2016 to 2019. Her research mainly focuses on smart soft materials and flexible sensors.

Wenan Zhang received the Ph. D. degree in Control Theory and Control Engineering from Zhejiang University of Technology, China, in 2010. He has been with Zhejiang University of Technology since 2010 where he is now a professor at Department of Automation. He was a senior research associate at Department of Manufacturing Engineering and Engineering Management, City University of Hong Kong, 2010–2011. He was awarded an Alexander von Humboldt Fellowship in 2011–2012. His current research interests include multi-sensor information fusion estimation and its applications. He has been serving as a subject editor for Optimal Control Applications and Methods from September 2016.

Dr. Xu Zhen received his Ph. D. degree from Zhejiang University in 2013. He joined in Zhejiang University as a distinguished researcher follow from 2017. He mainly focused on the research of graphene liquid crystal, two-dimensional macromolecular behavior and graphene fibers.

Hengjie Zhang received his B. S. degree in Anhui Polytechnic University in 2018. He is now studying for M. S. in Zhejiang University of Technology. His research interests involve design of flexible wearable sensors and microfluidic structures

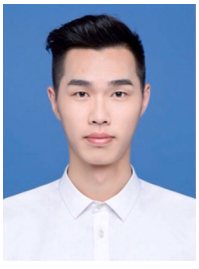

Hangcheng Qi received his B. S. degree in Wenzhou University in 2019. He is now studying for M. S. in Zhejiang University of Technology. His research interests involve flexible strain sensor and its applications in man-machine monitoring.

Prof. Aiping Liu received her Ph. D. degree in Material Science from the Harbin Institute of Technology in 2008. She worked as a postdoctoral research fellow at the Nanyang Technological University from 2009 to 2011 and a visiting scholar at the University of Texas at Austin from 2019 to 2020. She is currently a Professor in the Department of Physics at Zhejiang Sci-Tech University. Her research mainly focuses on the functional inorganic/organic material, with special emphasis on developing novel materials including graphene with sensing and actuation characteristic for wearable physical/chemical sensors and intelligent actuators.

Prof. Zheng Zhang is a full professor at Zhejiang University of Technology. He received his Ph. D. degree from Northwestern Polytechnical University in 2008. He performed research fellow at the City University of Hong Kong from 2008 to 2009. He became a lecturer at Zhejiang University of Technology in 2009 and an associate professor at Zhejiang University of Technology in 2013. His research interests focus on smart morphing structures, composite mechanics and numerical methods such as finite element method.

Prof. Huaping Wu received his Ph. D. degree in Engineering Mechanics from the Harbin Institute of Technology in 2009 and a Bachelor's degree from the Harbin Institute of Technology in 2002. He worked as a visiting scholar at the Kyoto University in 2014 and a postdoctoral research fellow at the City University of Hong Kong in 2012. He is currently a Professor in the School of Mechanical Engineering at Zhejiang University of Technology. His research mainly focuses on the mechanics of smart materials/structures, bionic machinery and bionic manufacturing, and flexible electronics devices.